

PAMELA's measurements of geomagnetic cutoff variations during the 14 December 2006 storm

O. Adriani^{1,2}, G. C. Barbarino^{3,4}, G. A. Bazilevskaya⁵, R. Bellotti^{6,7}, M. Boezio⁸,
 E. A. Bogomolov⁹, M. Bongi^{1,2}, V. Bonvicini⁸, S. Bottai², A. Bruno^{6,7,*}, F. Cafagna⁷,
 D. Campana⁴, P. Carlson¹⁰, M. Casolino^{11,12}, G. Castellini¹³, C. De Donato^{11,14},
 G. A. de Nolfo¹⁵, C. De Santis^{11,14}, N. De Simone¹¹, V. Di Felice^{11,16}, A. M. Galper¹⁸,
 A. V. Karelin¹⁸, S. V. Koldashov¹⁸, S. Koldobskiy¹⁸, S. Y. Krutkov⁹, A. N. Kvashnin⁵,
 A. Leonov¹⁸, V. Malakhov¹⁸, L. Marcelli^{11,14}, M. Martucci^{14,19}, A. G. Mayorov¹⁸,
 W. Menn²⁰, M. Mergé^{11,14}, V. V. Mikhailov¹⁸, E. Mocchiutti⁸, A. Monaco^{6,7}, N. Mori^{1,2},
 R. Munini^{8,17}, G. Osteria⁴, F. Palma^{11,14}, B. Panico⁴, P. Papini², M. Pearce¹⁰, P. Picozza¹⁴,
 M. Ricci¹⁹, S. B. Ricciarini^{2,13}, R. Sarkar^{21,22}, V. Scotti^{3,4}, M. Simon²⁰, R. Sparvoli^{11,14},
 P. Spillantini^{18,23}, Y. I. Stozhkov⁵, A. Vacchi⁸, E. Vannuccini², G. I. Vasilyev⁹,
 S. A. Voronov¹⁸, Y. T. Yurkin¹⁸, G. Zampa⁸ and N. Zampa⁸

¹ Department of Physics and Astronomy, University of Florence, I-50019 Sesto Fiorentino, Florence, Italy.

² INFN, Sezione di Florence, I-50019 Sesto Fiorentino, Florence, Italy.

³ Department of Physics, University of Naples “Federico II”, I-80126 Naples, Italy.

⁴ INFN, Sezione di Naples, I-80126 Naples, Italy.

⁵ Lebedev Physical Institute, RU-119991 Moscow, Russia

⁶ Department of Physics, University of Bari, I-70126 Bari, Italy.

⁷ INFN, Sezione di Bari, I-70126 Bari, Italy.

⁸ INFN, Sezione di Trieste, I-34149 Trieste, Italy.

⁹ Ioffe Physical Technical Institute, RU-194021 St. Petersburg, Russia.

¹⁰ KTH, Department of Physics, and the Oskar Klein Centre for Cosmoparticle Physics, AlbaNova University Centre, SE-10691 Stockholm, Sweden.

¹¹ INFN, Sezione di Rome “Tor Vergata”, I-00133 Rome, Italy.

¹² RIKEN, Advanced Science Institute, Wako-shi, Saitama, Japan.

¹³ IFAC, I-50019 Sesto Fiorentino, Florence, Italy.

¹⁴ Department of Physics, University of Rome “Tor Vergata”, I-00133 Rome, Italy.

¹⁵ Heliophysics Division, NASA Goddard Space Flight Center, Greenbelt, MD, USA.

¹⁶ Agenzia Spaziale Italiana (ASI) Science Data Center, Via del Politecnico snc, I-00133
Rome, Italy.

¹⁷ Department of Physics, University of Trieste, I-34147 Trieste, Italy.

¹⁸ National Research Nuclear University MEPhI, RU-115409 Moscow, Russia.

¹⁹ INFN, Laboratori Nazionali di Frascati, Via Enrico Fermi 40, I-00044 Frascati, Italy.

²⁰ Department of Physics, Universität Siegen, D-57068 Siegen, Germany.

²¹ Indian Centre for Space Physics, 43 Chalantika, Garia Station Road, Kolkata 700084,
West Bengal, India.

²² Previously at INFN, Sezione di Trieste, I-34149 Trieste, Italy.

²³ IAPS/INAF, I-00133 Rome, Italy.

* Corresponding author. E-mail address: alessandro.bruno@ba.infn.it.

ABSTRACT

Data from the Payload for Antimatter Matter Exploration and Light-nuclei Astrophysics (PAMELA) satellite experiment were used to measure the geomagnetic cutoff for high-energy ($\gtrsim 80$ MeV) protons during the 14 December 2006 geomagnetic storm. The variations of the cutoff latitude as a function of rigidity were studied on relatively short timescales, corresponding to spacecraft orbital periods (~ 94 min). Estimated cutoff values were compared with those obtained by means of a trajectory tracing approach based on a dynamical empirical modeling of the Earth’s magnetosphere. We found significant variations in the cutoff latitude, with a maximum suppression of ~ 7 deg at lowest rigidities during the main phase of the storm. The observed reduction in the geomagnetic shielding and its temporal evolution were related to the changes in the magnetospheric configuration, investigating the role of interplanetary magnetic field, solar wind and geomagnetic parameters. PAMELA’s results represent the first direct measurement of geomagnetic cutoffs for protons with kinetic energies in the sub-GeV and GeV region.

1. Introduction

The Cosmic Ray (CR) access to a specific location in the Earth’s magnetosphere is determined by the spatial structure and intensity of the geomagnetic field (Störmer 1955; Smart & Shea 2001), which is an highly dynamical system: its configuration is driven by the Solar Wind (SW) and by the interaction between the terrestrial and interplanetary fields, being compressed at the dayside and stretched toward the magnetotail on the nightside.

Major space weather phenomena are caused by Solar Energetic Particle (SEP)

events associated with explosive processes occurring in the solar atmosphere. SEPs can significantly increase the radiation dose rates compared with geomagnetically quiet times, disturbing satellite operations and producing hazardous effects to manned and robotic flight missions in the near-Earth environment, including aircrafts with their crew and passengers (Dyer et al. 2003), and influencing the atmospheric chemistry and dynamics (Danilov & Lastovicka 2001).

Large SEP events can strongly perturb the magnetosphere. In case of earthward-directed Coronal Mass Ejections (CMEs) or Co-rotating Interaction Regions (CIRs), disturbances can culminate in geomagnetic storms, characterized by a large transfer of the SW energy into the Earth’s magnetosphere, with significant changes in the currents, plasmas and fields (Leske et al. 2001). The reconnection of the field lines is more efficient when the Interplanetary Magnetic Field (IMF) is antiparallel to the terrestrial field on the dayside boundary of the magnetosphere (Dungey 1961; Akasofu 1981; Russell 2000). Intense geomagnetic storms can reduce the geomagnetic shielding and thus affect the planetary CR distribution (Dorman et al. 1973; Flueckiger et al. 1986; Smart et al. 2000).

An adequate description of the geomagnetic cutoff during SEP events has been the object of several studies based on multiple approaches, including spacecraft (Mazur et al. 1999; Leske et al. 2001; Ogliore et al. 2001; Birch et al. 2005) and ground-based (Rodger et al. 2006; Tyasto et al. 2013) observations, and calculations mainly based on tracing particles through models of the geomagnetic field (Smart & Shea 1985, 2001, 2003; Kress et al. 2010). Simplified empirical cutoff models have been developed, by parameterizing observations in terms of the Kp or Dst indices (Leske et al. 2001; Birch et al. 2005; Neal et al. 2013) or using multi-variable approaches (Dmitriev et al. 2010).

PAMELA’s measurements of relatively quiet magnetospheric cutoffs can be found in publications (Adriani et al. 2015c). In this work we present the measurement of the

cutoff variability during the strong geomagnetic storm on 14 December 2006, the last large CME-driven storm of the 23rd solar cycle.

2. The 14 December 2006 Geomagnetic Storm

On 13 December 2006 at 0214 UT, an X3.4/4B solar flare occurred in the active region NOAA 10930 (S06W23). This event also produced a full-halo CME with a sky plane projected speed of 1774 km s^{-1} (http://cdaw.gsfc.nasa.gov/CME_list/). The forward shock of the CME reached the Earth at about 1410 UT on 14 December causing a Forbush decrease of Galactic CR intensities that lasted for several days. The X1.5 flare (S06W46) at 2107 UT on 14 December gave start to a new growth of particle intensity, as recorded by PAMELA and other space-based detectors. The corresponding CME had a velocity of 1042 km s^{-1} . PAMELA’s measurements of the proton and helium fluxes during the 13–14 December 2006 events can be found in publications (Adriani et al. 2011).

Figure 1 reports the variations (12–18 December 2006) in the main IMF, SW and geomagnetic parameters. SW and IMF values were obtained from the high resolution (5-min) Omniweb database (<http://omniweb.gsfc.nasa.gov>), which provides in-situ observations time-shifted to the bow shock nose of the Earth (King & Papitashvili 2004). In particular, the interplanetary data for the considered time period are based on the measurements of the Advanced Composition Explorer (ACE) (Smith et al. 1998). The database was also exploited to derive the geomagnetic indices Kp , Dst and $Sym-H$ (at 3-hour, 1-hour, and 5-min resolutions, respectively), measured using ground-based magnetometers.

Some minor geomagnetic storms occurred on 12 December, while the time interval preceding the shock was characterized by a relatively low geomagnetic activity. The large

increase in the SW velocity V_{SW} on 14 December at ~ 1410 UT, associated with the leading edge of the CME, caused the Storm Sudden Commencement (SSC). The increased dynamical pressure P_{SW} resulted in a dramatic magnetospheric compression along with an intensification of the magnetopause current. The SSC, clearly visible in the time profiles of the geomagnetic indices, marked the beginning of the initial phase of the storm, which was characterized by intense fluctuations in P_{SW} and in all IMF components. In particular, B_z^{IMF} became positive after 1800 UT on 14 December and it continued to oscillate until the ~ 2300 UT, when the IMF intensity B_{tot}^{IMF} increased and B_z^{IMF} rapidly turned negative, while V_{SW} decreased. The main phase of the storm reached a maximum in the first hours of 15 December, followed by a slow (~ 3 days) recovery phase. The protracted large-amplitude (up to ~ 18 nT) southward IMF was associated with the magnetic cloud which caused the storm (Kataoka et al. 2009). Such large events are untypical of the intervals of low solar activity. An additional interplanetary shock, related to a less geo-effective CME, was registered on 16 December at ~ 1800 UT. Significant gaps in the ACE data are present after 1900 UT on 16 December.

3. PAMELA’s Observations

PAMELA is a space-based experiment designed for a precise measurement of the charged CRs (protons, electrons, their antiparticles and light nuclei) in the kinetic energy range from some tens of MeV up to several hundreds of GeV (Adriani et al. 2014). The Resurs-DK1 satellite, which hosts the apparatus, was launched into a semi-polar (70 deg inclination) and elliptical (350–610 km altitude) orbit on 15 June 2006. The instrument consists of a magnetic spectrometer equipped with a silicon tracking system, a time-of-flight system shielded by an anticoincidence system, an electromagnetic calorimeter and a neutron detector (Picozza et al. 2007). Details about apparatus performance, proton

selection, detector efficiencies and experimental uncertainties can be found elsewhere (see e.g. Adriani et al. (2013)).

PAMELA is providing comprehensive observations of the interplanetary (Adriani et al. 2013, 2015d) and magnetospheric (Adriani et al. 2015b,c) radiation in the near-Earth environment. In particular, PAMELA is able to accurately measure the SEP events during solar cycles 23 and 24 (Adriani et al. 2011, 2015a), including energetic spectra and pitch angle distributions (Bruno et al. 2015a) in a wide interval, bridging the low energy data by in-situ spacecrafts and the Ground Level Enhancement (GLE) data by the worldwide network of neutron monitors.

3.1. Magnetic Coordinates

Data were analyzed in terms of Altitude Adjusted Corrected GeoMagnetic (AACGM) coordinates, developed to provide a realistic description of high latitude regions by accounting for the multipolar geomagnetic field. They are defined such that all points along a magnetic field line have the same geomagnetic latitude and longitude, so that they are closely related to invariant magnetic coordinates (Baker & Wing 1989; Gustafsson et al. 1992; Heres & Bonito 2007). The AACGM system coincides with the standard Corrected GeoMagnetic (CGM) system (Brekke et al. 1997) at the Earth’s surface. The computation is based on the IGRF-11 model (Finlay et al. 2010), which employs a global spherical harmonic implementation of the main magnetic field; AACGM latitudes at PAMELA’s orbit are not significantly affected by the inclusion of external geomagnetic sources.

Alternatively, following the standard approach, cutoff observations were expressed as a function of the McIlwain’s L parameter (McIlwain 1966). In a dipole, L numerically approximates the radius (measured in R_E) where a geomagnetic field line crosses the

equator. The invariant latitude Λ_{inv} of a location, derived from L by the relation: $\cos\Lambda_{inv} = L^{-1/2}$, represents a particularly useful parameter for the investigation of high latitude phenomena.

3.2. Evaluation of Geomagnetic Cutoff Latitudes

The lowest magnetic latitude to which a charged CR particle can penetrate the Earth’s magnetic field is known as its *cutoff latitude* and is a function of the particle rigidity (R = momentum/charge). Alternatively, a *cutoff rigidity* can be associated with a given location in the magnetosphere, corresponding to the minimum rigidity needed to access to the considered position. Some complications arise from the presence of the Earth’s solid body (together with its atmosphere): both “allowed” and “forbidden” bands of CR particle access are present in the so-called “penumbra” region (Cooke et al. 1991). Cutoff values are in general a function of particle direction of arrival and geomagnetic activity. Due to the narrow (~ 20 deg) field of view of PAMELA, with its major axis mostly oriented toward the zenith, the measured CR fluxes correspond to approximately vertical directions.

The algorithm used to evaluate cutoff latitudes from the PAMELA data (Bruno et al. 2015b) is similar to one developed by Leske et al. (2001), using the low-energy proton and alpha particle measurements made by the Solar Anomalous and Magnetospheric Particle Explorer (SAMPEX) spacecraft. For each rigidity bin, a mean flux was obtained by averaging fluxes measured at latitudes higher than $\Lambda_{min} = \cos^{-1}(R[GV]/20)^{1/4}$ deg. Λ_{min} , employed to improve the statistics at high rigidities, represents a rigidity dependent upper cutoff developed to avoid penumbral effects, and it was derived by using proton data acquired by PAMELA during relatively quiet geomagnetic conditions (Adriani et al. 2015c).

To support the analysis results, cutoff latitudes were also numerically modeled with

back-tracing techniques (Bruno et al. 2015a,c). Using the spacecraft ephemeris data, and the particle rigidity and direction provided by the tracking system, trajectories of all selected protons were reconstructed in the Earth’s magnetosphere by means of a tracing program based on Smart & Shea (2000) and implementing a realistic semi-empirical description of internal and external geomagnetic field sources (see Section 3.3.2). In order to discard geomagnetically trapped protons (Adriani et al. 2015b) and low energy albedo protons (Adriani et al. 2015c) in the equatorial regions, while saving significant computational time, only protons with rigidities higher than $10/L^3$ GV were selected. Trajectories were back propagated from the measurement location until they escaped the model magnetosphere boundaries (interplanetary CRs) or they reached an altitude of 40 km (albedo CRs). Then, at a given rigidity, the *modeled* cutoff latitude was evaluated as the latitude where the interplanetary and albedo flux intensities were equal.

Accounting for the statistical limitations, the calculation was performed for 18 rigidity logarithmic bins covering the interval 0.39–7.47 GV and the final cutoff values were derived by fitting PAMELA’s observations averaged over single orbital periods (~ 94 min), including two cutoff measurements (entering and exiting the polar caps) in both magnetic hemispheres. The relationships used to fit cutoff latitude data were obtained by inverting the formulas developed to describe cutoff rigidities:

$$R(\Lambda) = a_{\Lambda} \cdot \cos^4 \Lambda - b_{\Lambda}, \quad (1)$$

$$R(L) = a_L/L^2 - b_L, \quad (2)$$

as a function of AACGM (or invariant) latitude Λ and L -shell respectively, with $(a_{\Lambda}, b_{\Lambda})$ and (a_L, b_L) the corresponding fitting parameters (Adriani et al. 2015c). Such a parameterization, which takes into account the magnetospheric effects at high latitudes, was introduced by Ogliore et al. (2001) to reproduce CR nuclei observations made by the SAMPEX mission. In general, the fit results can vary up to a factor 10% at equatorial and

mid-latitude locations due to the non-dipole terms in the geomagnetic field (Smart & Shea 2005).

3.3. Results

Figure 2 shows the geomagnetic cutoff latitudes measured by PAMELA for different rigidity bins (color code), between 12 and 18 December 2006. Cutoff results are reported for both AACGM (top) and invariant (bottom) latitudes. Each point denotes the cutoff latitude value averaged over a single spacecraft orbit (2 full polar passes); the error bars include the statistical uncertainties of the measurement. In a few of cases data points are missing because the numerical algorithm used to evaluate cutoff latitudes returned no cutoff or a bad cutoff value, due to limited statistics. The gap in the PAMELA data from 1000 UT on 13 December until 0914 UT on 14 December was related to an onboard system reset of the satellite.

The evolution of the 14 December magnetic storm followed the typical scenario in which the cutoff latitudes move equatorward as a consequence of a CME impact on the magnetosphere with an associated transition to southward B_z^{IMF} . The maximum cutoff suppression was observed during the storm’s main phase at about 0300 UT on 15 December. The registered deviation with respect to quiet geomagnetic conditions decreases with increasing rigidity, with a ~ 7 deg maximum suppression for the lowest rigidity bin (0.39–0.46 GV).

Globally mapped cutoffs in geographic coordinates at mean PAMELA altitude (475 km) are shown in Figure 3. The maps were derived from fitted results by evaluating cutoff rigidities (extrapolated down to 0 GV) as a function of L through Equation 2, and averaging PAMELA data over the two hemispheres and over the longitudes. The top-left

panel displays cutoffs measured on 14 December during the orbital interval 1344–1518 UT, including the shock arrival on the magnetosphere; the top-right panel report the results on 15 December between 0216 and 0350 UT, at the maximum registered cutoff suppression. Bottom panels show the corresponding cutoff differences with respect to geomagnetically quiet conditions. Significant discrepancies were found in both cases: the rigidity cutoff suppression after the shock arrival is ~ 0.33 GV at highest magnetic latitudes, about a third of the maximum deviation registered in the main phase of the storm (~ 1 GV).

3.3.1. Correlations with Interplanetary and Geomagnetic Parameters

Figure 4 reports the variations in the measured cutoff latitudes in the lowest rigidity bin (0.39–0.46 GV), compared to the time profiles of IMF (B_y^{IMF} , B_z^{IMF} components and B_{tot}^{IMF} total intensity), SW (dynamical pressure P_{SW} , velocity V_{SW} and density d_{SW}) and geomagnetic (Kp , Dst and $Sym-H$ indices) parameters. Correlation coefficients were estimated by interpolating and averaging Omniweb data (characterized by different time resolutions) over PAMELA orbital periods (~ 94 min). The results of the analysis of the correlations are shown in Figure 5. Partial correlation values for the three (initial, main, recovery) storm phases are reported in Table 1, along with the total correlation coefficients. Values in bold correspond to a strong correlation (≥ 0.80) or anti-correlation (≤ -0.80).

During the initial phase (14 December, 1410–2300 UT), the most geo-effective parameters were P_{SW} , d_{SW} and B_{tot}^{IMF} ; a good correlation was observed for Dst and $Sym-H$. In the main phase (lasting up to ~ 0400 UT on 15 December), very pronounced interplanetary effects were exerted by B_y^{IMF} , B_{tot}^{IMF} , P_{SW} and d_{SW} , while B_z^{IMF} was moderately correlated. Note that SW parameters were anti-correlated and correlated with the cutoff latitude variations in the initial and the main phases, respectively. Furthermore, a significant correlation was shown by Dst and $Sym-H$; however, the Dst index was

Phase	B_y^{IMF}	B_z^{IMF}	B_{tot}^{IMF}	P_{SW}	V_{SW}	d_{SW}	Kp	Dst	$Sym-H$
Initial	0.03	-0.28	-0.70	-0.76	-0.41	-0.74	-0.56	0.75	0.73
Main	-0.95	0.68	-0.93	0.93	0.35	0.94	-0.69	0.89	0.93
Recovery	-0.74	0.94	-0.84	-0.28	-0.73	-0.08	-0.94	0.94	0.91
All	-0.51	0.81	-0.82	-0.16	-0.52	-0.12	-0.89	0.74	0.80

Table 1: Correlation coefficients between measured cutoff latitudes (0.39–0.46 GV) and main IMF, SW and geomagnetic parameters, during the three different (initial, main, recovery) storm phases and the whole storm (all).

characterized by a very slow decrease between 0300–0700 UT on 15 December, and the maximum cutoff suppression in PAMELA data was observed about 4 hours before the Dst minimum (-162 nT). Instead, Kp changes were much less correlated due to the coarser resolution. Finally, the recovery phase was characterized by a strong correlation with B_{tot}^{IMF} and, especially, with B_z^{IMF} and all the three geomagnetic indices. B_y^{IMF} and V_{SW} were also quite geo-effective. Note that the time period considered for the recovery phase is limited to 1900 UT on 16 December, due to the gaps in ACE data. In general, as demonstrated in Figure 5, the shapes of the time variations in the PAMELA’s cutoff measurements were strongly correlated with B_z^{IMF} , B_{tot}^{IMF} , $Sym-H$ and especially Kp . A less significant correlation was observed for Dst : while the Kp changes appeared to lead the cutoff suppressions, Dst was found to respond with some delay (see Figure 4), in agreement with previous studies (Leske et al. 2001; Neal et al. 2013).

3.3.2. Comparison with Modeled Cutoffs

Figure 6 reports the comparison between measured and modeled cutoff latitudes during the geomagnetic storm, for the lowest rigidity bin (0.39–0.46 GV). Modeled cutoffs were

obtained by using the IGRF-11 and the Tsyganenko & Sitnov (2005) (TS05) models for the description of internal and external geomagnetic field sources, respectively. The TS05 model is a high resolution dynamical model of the storm-time magnetosphere, based on recent satellite measurements. The model input consists in B_y^{IMF} , B_z^{IMF} , P_{SW} and Dst ; 6 additional supplied parameters describe the strength of the symmetric ring current, the partial ring current, the Birkeland 1 and 2 currents, and two different tail current systems. Alternatively, the less sophisticated Tsyganenko (1996) (T96) model was used.

PAMELA data (black) are well reproduced by the TS05 model (red) within statistical errors: on average, modeled cutoff latitudes are $\sim 0.31 \pm 1.22$ deg equatorward shifted; small mean differences can be observed in the initial and recovery phases of the storm (about -0.32 ± 1.25 deg and -0.43 ± 1.20 deg, respectively), while the modeled cutoffs are $\sim 1.07 \pm 1.34$ deg poleward in the main phase; overall, the maximum deviation from PAMELA's cutoffs is ~ 1.3 deg.

On the other hand, the cutoff latitudes estimated with the T96 model (blue) are systematically ($\sim 1.49 \pm 1.30$ deg) equatorward of the PAMELA's observations during all storm phases, with a larger maximum deviation (~ 2.8 deg). This is not unexpected since the magnetospheric description provided by the T96 model is not adequate in the case of intense geomagnetic activity, overestimating storm effects (Desorgher et al. 2009).

4. Summary and Conclusions

In this study we have taken advantage of the proton data of the PAMELA satellite experiment to perform a measurement of the geomagnetic cutoff variations during the long lasting storm on 14 December 2006. The arrival of the 13 December CME caused a strong perturbation of the local radiation environment, affecting the planetary CR distribution.

The evolution of the consequent geomagnetic storm followed the typical scenario in which the cutoff latitudes move equatorward as a consequence of a magnetic cloud impact on the Earth’s magnetosphere with an associated transition to southward IMF. A significant reduction in the geomagnetic shielding was observed, with a maximum cutoff latitude suppression of about 7 deg at lowest rigidities. Such large CME-driven storms are relatively rare during the intervals of low solar activity. The variability of the cutoff latitude as a function of rigidity was studied on relatively short timescales, corresponding to single spacecraft orbits (~ 94 min). Measured cutoff variations were related to the changes in the magnetosphere configuration, investigating the role of IMF, SW and geomagnetic parameters. In particular, we found an high correlation with the variations of B_z^{IMF} , B_{tot}^{IMF} and the geomagnetic activity as measured by the Kp index and, to a lesser extent, by the $Sym-H$ index. Finally, results were compared with those obtained with back-tracing techniques based on a realistic semi-empirical modeling of the magnetosphere. PAMELA’s observations represent the first direct measurement of geomagnetic cutoffs for protons with kinetic energies from ~ 80 MeV to several GeV.

We acknowledge support from The Italian Space Agency (ASI), Deutsches Zentrum für Luftund Raumfahrt (DLR), The Swedish National Space Board, The Swedish Research Council, The Russian Space Agency (Roscosmos) and The Russian Scientific Foundation.

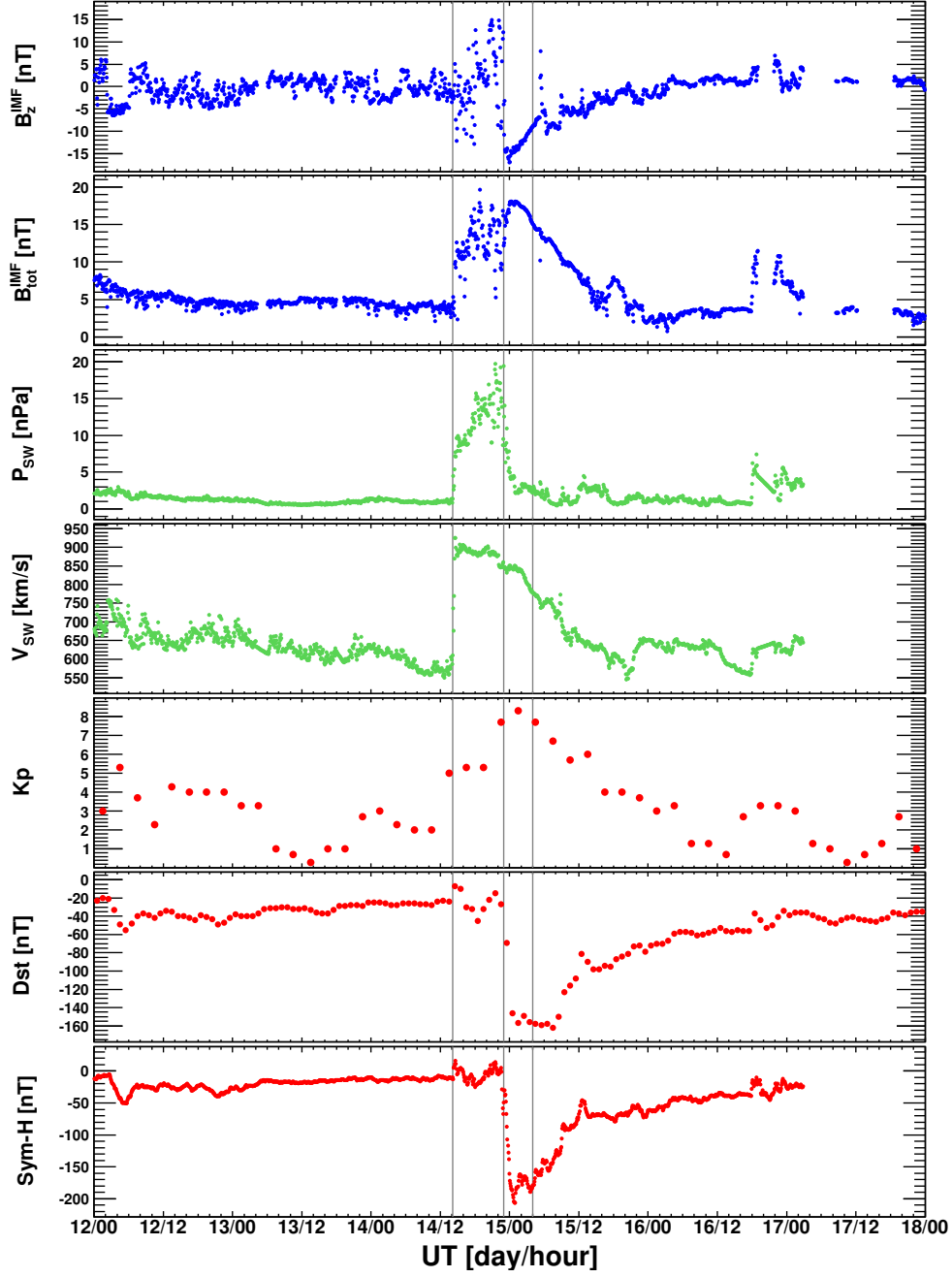


Fig. 1.— Time profiles of the main IMF (B_z^{IMF} and B_{tot}^{IMF} ; blue), solar wind (P_{SW} and V_{SW} ; green) and geomagnetic (Kp , Dst , $Sym-H$; red) parameters between 12–18 December 2006. The vertical lines mark the beginning of the storm initial, main and recovery phases, respectively.

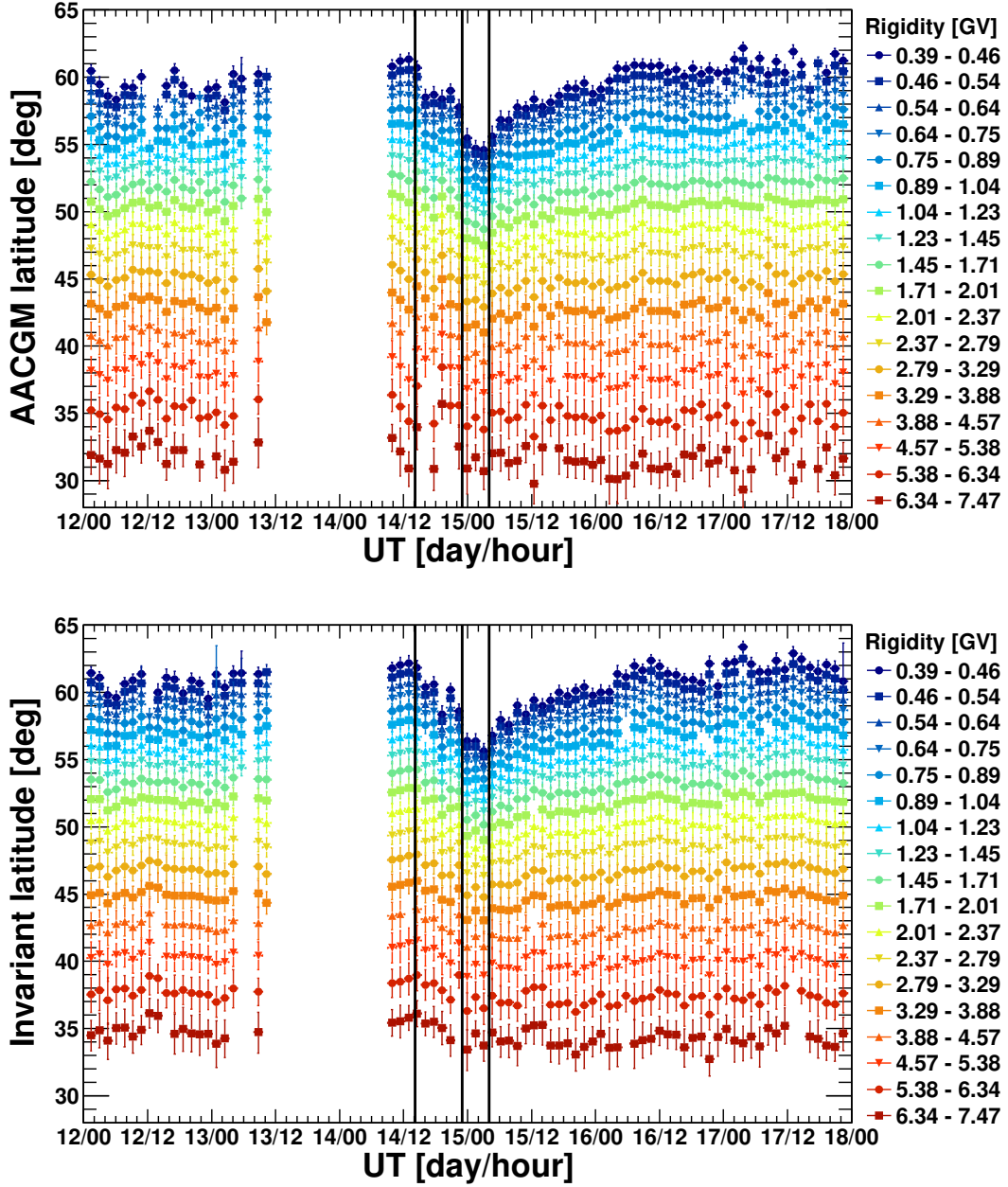


Fig. 2.— Time profile of the geomagnetic cutoff latitudes measured by PAMELA, for different rigidity bins (color code). Cutoff results are reported for both AACGM (top) and invariant (bottom) latitudes. The vertical lines mark the beginning of the storm initial, main and recovery phases, respectively.

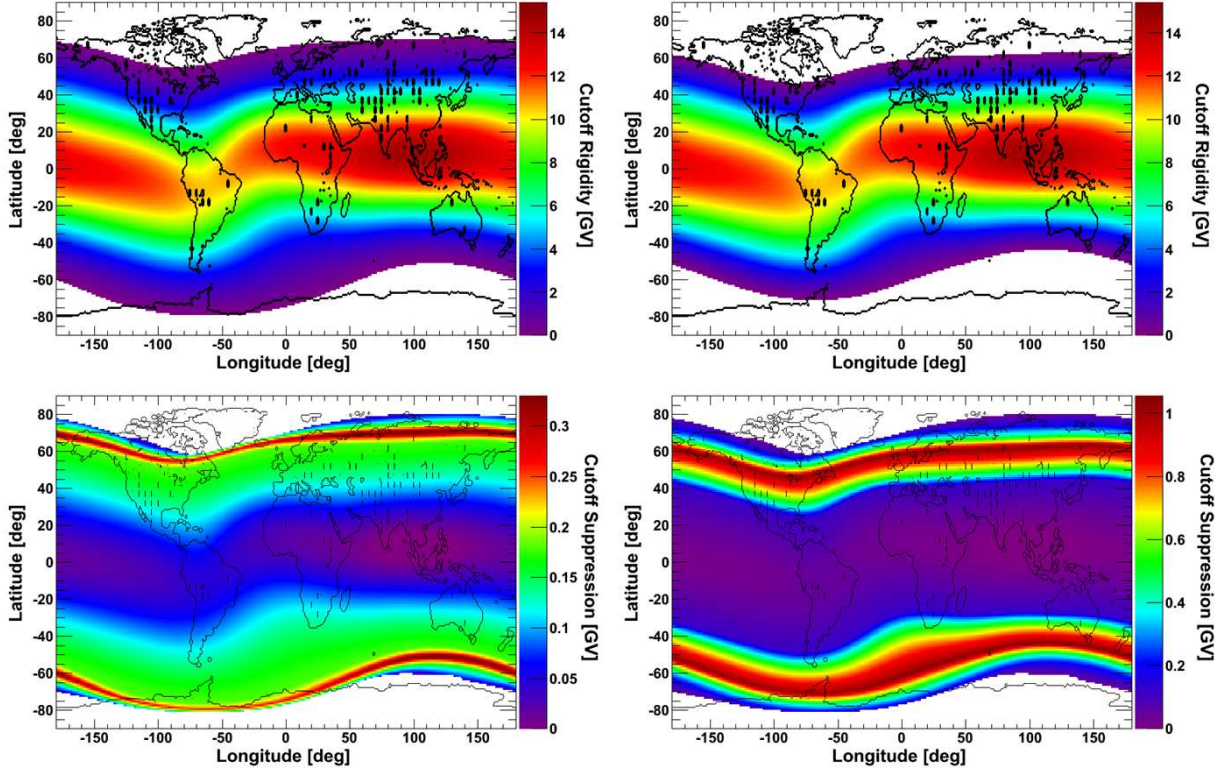


Fig. 3.— Cutoff rigidity maps evaluated at the shock arrival (top-left), and at the time of maximum cutoff suppression (top-right). Bottom panels show the corresponding cutoff decrease with respect to geomagnetically quiet conditions.

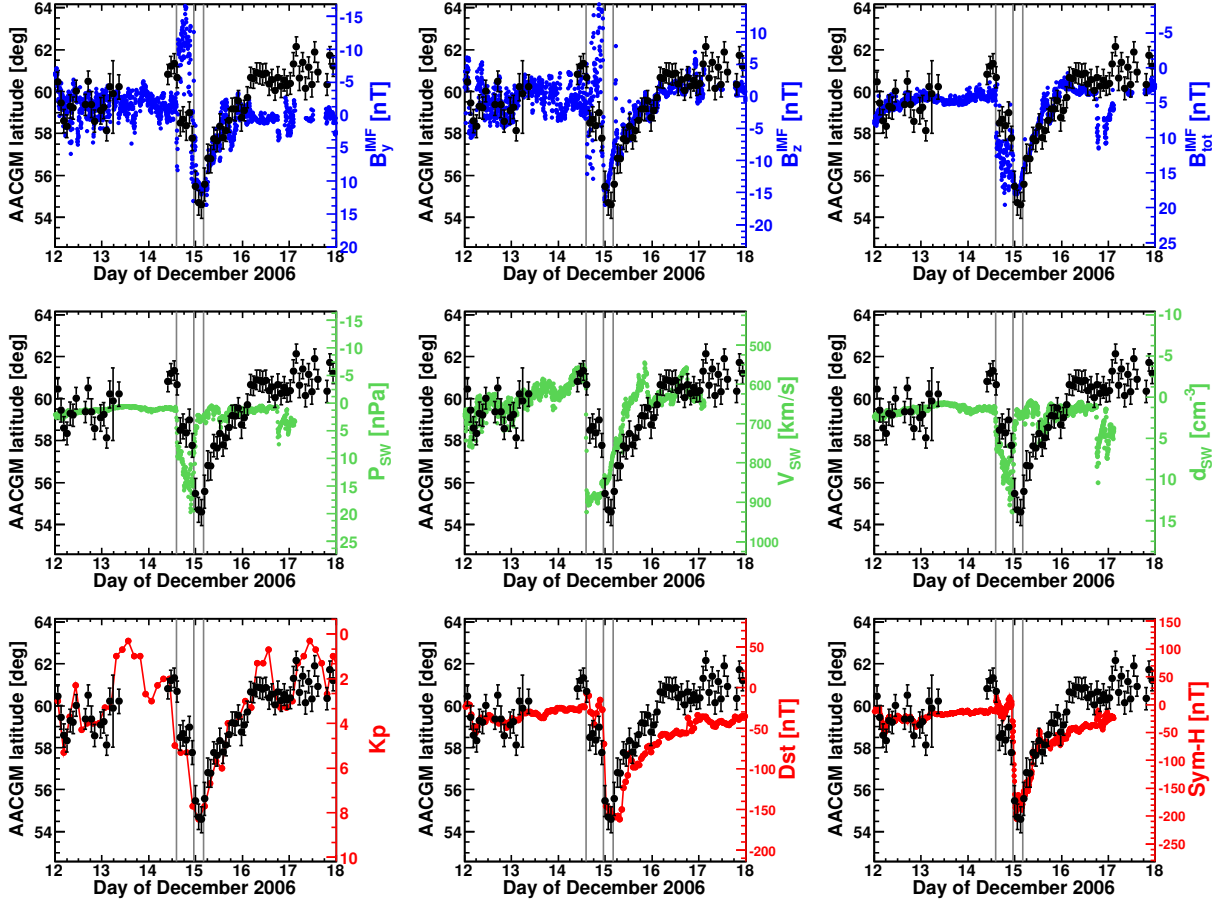


Fig. 4.— Time profiles of the IMF (B_y^{IMF} , B_z^{IMF} and B_{tot}^{IMF} ; blue), solar wind (P_{sw} , V_{sw} and d_{sw} ; green) and geomagnetic (Kp , Dst , $Sym-H$; red) parameters, compared with the variations in measured cutoff latitudes (0.39–0.46 GV; black). The vertical lines mark the beginning of the storm initial, main and recovery phases, respectively.

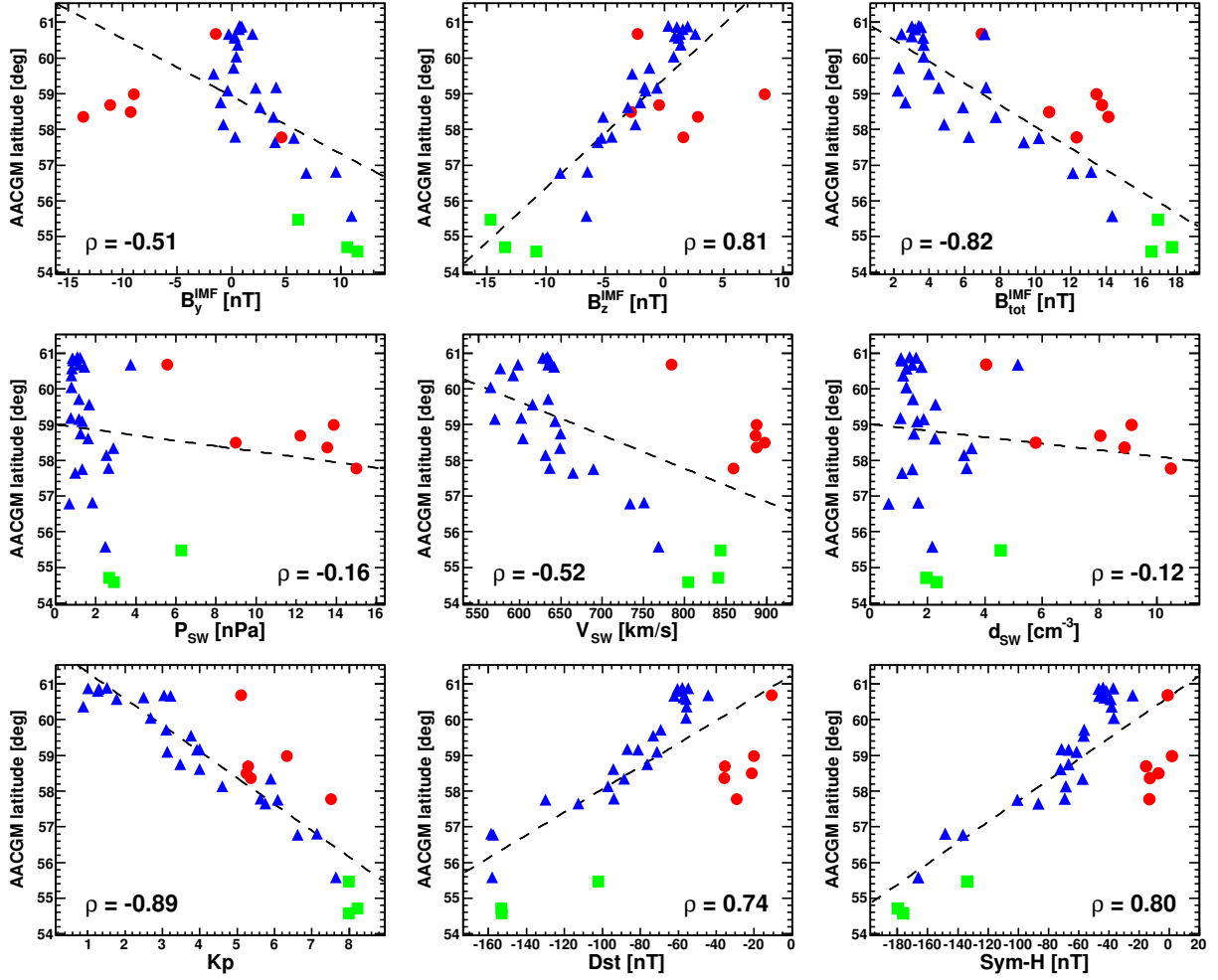


Fig. 5.— Correlation between measured cutoff latitudes in the 0.39–0.46 GV rigidity bin (Y-axis) and main IMF, SW and geomagnetic parameters (X-axis). Orbital-averaged data during the three (initial, main, recovery) storm phases are indicated by red circles, green squares and blue triangles, respectively. The corresponding total correlation coefficient ρ is reported in each panel.

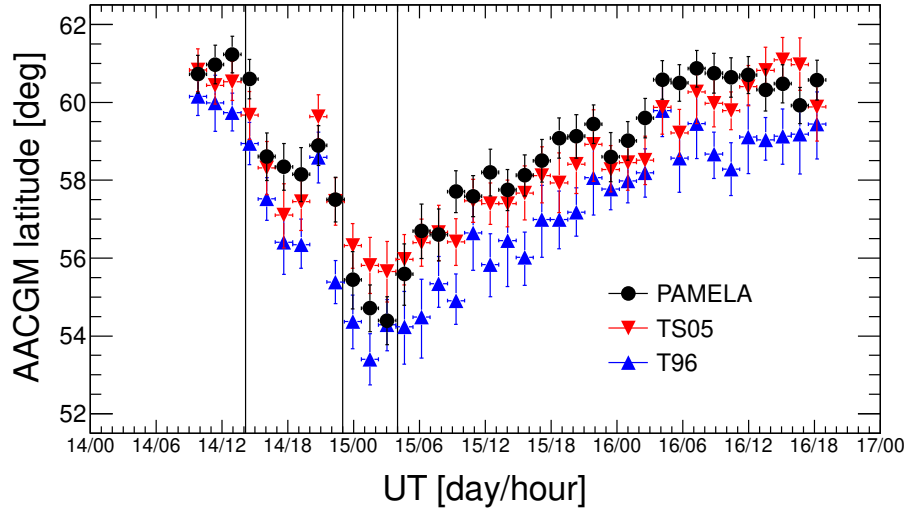


Fig. 6.— Comparison between measured (black squares) and modeled (blue triangles - T96 model; red circles - TS05 model) cutoff variations in the lowest rigidity interval: 0.39–0.46 GV. The vertical lines mark the beginning of the storm initial, main and recovery phases, respectively.

REFERENCES

- Adriani, O., et al. (2011), Observations of the 2006 December 13 and 14 solar particle events in the 80 MeV n^{-1} – 3 GeV n^{-1} range from space with the PAMELA detector, *ApJ* 742:102, doi:10.1088/0004-637X/742/2/102.
- Adriani, O., et al. (2013), Time dependence of the proton flux measured by PAMELA during the 2006 July – 2009 December solar minimum, *ApJ* 765:91.05205, doi:10.1088/0004-637X/765/2/91.
- Adriani, O., et al. (2014), The PAMELA Mission: Heralding a new era in precision cosmic ray physics, *Physics Reports*, 544, 4, 323–370, doi:10.1016/j.physrep.2014.06.003.
- Adriani, O., et al. (2015a), PAMELA’s Measurements of Magnetospheric Effects on High Energy Solar Particles, *ApJ* 801 L3, doi:10.1088/2041-8205/801/1/L3.
- Adriani, O., et al. (2015b), Trapped Proton Fluxes at Low Earth Orbits Measured by the PAMELA Experiment, *ApJ* 799 L4, doi:10.1088/2041-8205/799/1/L4.
- Adriani, O., et al. (2015c), Re-entrant albedo proton fluxes measured by the PAMELA experiment, *J. Geophys. Res. Space Physics*, 120, doi:10.1002/2015JA021019.
- Adriani, O., et al. (2015d), Time Dependence of the e- Flux Measured by PAMELA during the July 2006-December 2009 Solar Minimum, *ApJ*, 810, 142, doi:10.1088/0004-637X/810/2/142.
- Akasofu, S.-I. (1981), Energy coupling between the solar wind and the magnetosphere, *Space Sci. Rev.*, 28, 121–190, doi:10.1007/BF00218810.
- Baker, K. B., and S. Wing (1989), A new magnetic coordinate system for conjugate studies at high latitudes, *J. Geophys. Res.*, 94, 9139–9143, doi:10.1029/JA094iA07p09139.

- Birch, M. J., et al. (2005), Variations in cutoff latitude during selected solar energetic proton events, *J. Geophys. Res.*, *110*, A07221, doi:10.1029/2004JA010833.
- Brekke, A. (1997), *Physics of the Upper Polar Atmosphere*, Wiley, New York, 127–145, doi:10.1007/978-3-642-27401-5.
- Bruno, A., et al. (2015a), Solar energetic particle events: trajectory analysis and flux reconstruction with PAMELA, *Proc. 34th Intl. Cosmic Ray Conf.*, PoS(ICRC2015)085.
- Bruno, A., et al. (2015b), PAMELA’s measurements of geomagnetic cutoff variations during solar energetic particle events, *Proc. 34th Intl. Cosmic Ray Conf.*, PoS(ICRC2015)287.
- Bruno, A., et al. (2015c), PAMELA’s measurements of geomagnetically trapped and albedo protons, *Proc. 34th Intl. Cosmic Ray Conf.*, PoS(ICRC2015)288.
- Cooke, D. J. , et al. (1991), On cosmic ray cut-off terminology, *Il Nuovo Cimento*, *14C*, 213, doi:10.1007/BF02509357.
- Danilov, A. D., and J. Lastovicka (2001), Effects of geomagnetic storms on the ionosphere and atmosphere, *Int. J. Geomagn. Aeron.* *2*(3): 209-224.
- Desorgher, L., et al. (2009), Comparison of Earth’s magnetospheric magnetic field models in the context of cosmic ray physics, *Acta Geophys.*, *57* (1), 75–87, doi:10.2478/s11600-008-0065-3.
- Dmitriev, A. V., P. T. Jayachandran, and L.-C. Tsai (2010), Elliptical model of cutoff boundaries for the solar energetic particles measured by POES satellites in December 2006, *J. Geophys. Res.*, *115*, A12244, doi:10.1029/2010JA015380
- Dorman, L. I., V. S. Smirnov, and M. I. Tyasto (1973), *Cosmic rays in the Earth’s magnetic field*, Washington, NASA, Springfield, Va. 423.

- Dungey, J. W. (1961), Interplanetary magnetic field and the auroral zones, *Phys. Rev. Lett.*, *APS*, 6, 47–48, doi:10.1103/PhysRevLett.647.
- Dyer, C. S., et al. (2003), Calculations and observations of solar particle enhancements to the radiation environment at aircraft altitudes, *Adv. Space Res.*, 32(1), 81–93, doi:10.1016/S0273-1177(03)90374-7.
- Finlay, C. C., et al. (2010), International Geomagnetic Reference Field: the eleventh generation, *Geophysical Journal International*, 183: 1216–1230, doi:10.1111/j.1365-246X.2010.04804.x.
- Flueckiger, E. O., D. F. Smart, and M. A. Shea (1986), A procedure for estimating the changes in cosmic ray cutoff rigidities and asymptotic directions at low and middle latitudes during periods of enhanced geomagnetic activity, *J. Geophys. Res.* 91 (A7), 7925–7930, doi:10.1029/JA091iA07p07925.
- Gustafsson, G., N. E. Papitashvili, and V. O. Papitashvili (1992), A revised corrected geomagnetic coordinate system for epochs 1985 and 1990, *J. Atmos. Terr. Phys.*, 54, 1609–1631, doi:10.1016/0021-9169(92)90167-J.
- Heres, W., and N. A. Bonito (2007), Alternative method of computing altitude adjustment corrected geomagnetic coordinates as applied to IGRF epoch 2005, *Sci. Rep. AFRL-RV-HA-TR-2007-1190*, Atmospheric and Environmental Research (AER), Inc., Lexington, Mass.
- Kataoka, R., et al (2009), Three-dimensional MHD modeling of the solar wind structures associated with 13 December 2006 coronal mass ejection, *J. Geophys. Res.*, 114, A10102, doi:10.1029/2009JA014167.
- King, J. H., and N. E. Papitashvili (2004), Solar wind spatial scales in and comparisons of

- hourly Wind and ACE plasma and magnetic field data, *J. Geophys. Res.*, *110*, A2, A02209, doi:10.1029/2004JA010649.
- Kress, B. T., C. J. Mertens, and M. Wiltberger (2010), Solar energetic particle cutoff variations during the 29–31 October 2003 geomagnetic storm, *Space Weather*, *8*, S05001, doi:10.1029/2009SW000488.
- Leske, R. A., R. A. Mewaldt, E. C. Stone, T. T. von Rosenvinge (2001), Observations of geomagnetic cutoff variations during solar energetic particle events and implications for the radiation environment at the space station, *J. Geophys. Res.*, *106*, 30,011–30,022, doi:10.1029/2000JA000212.
- Mazur, J. E., G. M. Mason, M. D. Looper, R. A. Leske and R. A. Mewaldt (1999), Charge states of solar energetic particles using the geomagnetic cutoff technique: SAMPEX measurements in the 6 November 1997 solar particle event, *Geophys. Res. Lett.*, *26*, 2, 173–176, doi:10.1029/1998GL900075.
- McIlwain, C. (1966), Magnetic coordinates, *Space Sci. Rev.* *5*, 585–589.
- Neal, J. J., C. J. Rodger, and J. C. Green (2013), Empirical determination of solar proton access to the atmosphere: Impact on polar flight paths, *Space Weather*, *11*, 420–433, doi:10.1002/swe.20066.
- Ogliore, R. C., R. A. Mewaldt, R. A. Leske, E. C. Stone, T. T. von Rosenvinge (2001), A Direct Measurement of the Geomagnetic Cutoff for Cosmic Rays at Space Station Latitudes, *Proc. 27th Intl. Cosmic Ray Conf.*, *10*, 4112–4115.
- Picozza, P., et al. (2007), PAMELA – A payload for antimatter matter exploration and light–nuclei astrophysics, *Astropart. Phys.*, *27*, 296–315, doi:10.1016/j.astropartphys.2006.12.002.

- Rodger, C. J., et al. (2006), Dynamic geomagnetic rigidity cutoff variations during a solar proton event, *J. Geophys. Res.*, *111*, A04222, doi:10.1029/2005JA011395.
- Russell, C. T. (2000), The solar wind interaction with the Earth’s magnetosphere: a tutorial, *IEEE Trans. Plasma Sci.* *28*, 6, 1818–1830, doi:10.1109/27.902211.
- Smart, D. F., and M. A. Shea (1985), A simplified model for timing the arrival of solar flare-initiated shocks, *J. Geophys. Res.*, *90*, 183–190, doi:10.1029/JA090iA01p00183.
- Smart, D. F., and M. A. Shea (2000), Final Report, Grant NAG5–8009, Center for Space Plasmas and Aeronomic Research, The University of Alabama in Huntsville.
- Smart, D. F., and M. A. Shea (2001), A comparison of the tsyganenko model predicted and measured geomagnetic cutoff latitudes, *Adv. Space Res.*, *28*, 1733–1738, doi:10.1016/S0273-1177(01)00539-7.
- Smart, D. F., and M. A. Shea (2003), The space-developed dynamic vertical cutoff rigidity model and its applicability to aircraft radiation dose, *Adv. Space Res.*, *32*(1), 103–108, doi:10.1016/S0273-1177(03)90376-0.
- Smart, D. F., and M. A. Shea (2005), A review of geomagnetic cutoff rigidities for Earth-orbiting spacecraft, *Adv. Space Res.*, *36*, 2012–2020, doi:10.1016/j.asr.2004.09.015.
- Smart, D. F., M. A. Shea, and E. O. Flueckiger (2000), Magnetospheric models and trajectory computations, *Space Sci. Rev.* *93*, 271–298, doi:10.1023/A:1026556831199.
- Smith, C. W., et al. (1998), The ACE Magnetic Fields Experiment, *Space Sci. Rev.* *86*, 611, doi:10.1023/A:1005092216668.
- Störmer, C. (1955), *The Polar Aurora*, Oxford Univ. Press, New York.

- Tsyganenko, N. A. (1996), Effects of the solar wind conditions on the global magnetospheric configuration as deduced from data-based field models, *Proc. ICS-3 Conference on Substorms*, Eur. Space Agency Spec. Publ., ESA SP-389, 181
- Tsyganenko, N. A., and M. I., Sitnov (2005), Modeling the dynamics of the inner magnetosphere during strong geomagnetic storms, *J. Geophys. Res.*, *110*, A03208, doi:10.1029/2004JA010798.
- Tyasto, M. I., et al. (2013), Variations in cosmic ray cutoff rigidities during the great geomagnetic storm of November 2004, *Adv. Space Res.*, *51*, 1230–1237, doi:10.1016/j.asr.2012.10.025.